

Geophysical Research Letters



RESEARCH LETTER

10.1029/2020GL091722

Key Points:

- Cross-shore sediment transport in the nearshore can be unstable in the alongshore direction
- The morphodynamic instability can develop only for beach profiles above the equilibrium profile
- This instability could explain transverse finger bar formation at beaches with sediment excess

Supporting Information:

Supporting Information may be found in the online version of this article.

Correspondence to:





F. Ribas,
albert.falques@upc.edu

Citation:

Falqués, A., Ribas, F., Mujal-Colilles, A., & Puig-Polo, C. (2021). A new morphodynamic instability associated with cross-shore transport in the nearshore. *Geophysical Research Letters*, 48, e2020GL091722. <https://doi.org/10.1029/2020GL091722>

Received 16 NOV 2020
Accepted 28 MAY 2021

A New Morphodynamic Instability Associated With Cross-Shore Transport in the Nearshore

A. Falqués¹ , F. Ribas¹ , A. Mujal-Colilles² , and C. Puig-Polo³ 

¹Physics Department, Universitat Politècnica de Catalunya, Campus Diagonal Nord, Barcelona, Spain, ²Department of Nautical Sciences and Engineering, Universitat Politècnica de Catalunya, Barcelona, Spain, ³Department of Civil and Environmental Engineering, Universitat Politècnica de Catalunya, Barcelona, Spain

Abstract The existing theory for shore-transverse rhythmic sand bars relies on morphodynamic instabilities involving the wave-driven longshore current and rip currents. Intriguingly, transverse finger bars are common on coasts with sediment excess, something not related to those currents. Here we show that, if the actual beach profile is above the equilibrium profile, cross-shore transport can induce an instability triggered by onshore transport together with wave refraction by the emerging bars. We use a numerical model that filters out the dynamics associated to longshore and rip currents but includes a simplified version of cross-shore transport and is able to reproduce the formation of shore-transverse bars. The alongshore spacing scales with the wavelength of the incident waves and the cross-shore extent is approximately equal to the distance from shore to the depth of closure. The modeled bars compare qualitatively well with observations at El Trabucador back-barrier beach (Ebro delta, Western Mediterranean Sea).

Plain Language Summary Beaches sometimes exhibit sand ridges (bars) nearly perpendicular to shore that tend to be quite regularly spaced alongshore. Their spacing and cross-shore extent range from tens to thousands of meters. Intriguingly, these bars develop preferably at beaches with an abundant supply of sand such as delta barrier beaches, barrier islands and estuaries. Here we provide a possible explanation. Due to the sand excess, the bed in these beaches is very flat, the tendency for the sand to move downslope is very weak and the waves push the sand onshore. On the other hand, waves refract, that is, their crest tip on deeper water propagates faster than the tip on shallower water. As a result, they turn toward shallower areas and, thus, the onshore movement of the sand is deflected toward incipient shoals and accumulates there. This causes more intense wave refraction, which in turn brings more sand to the shallows, and so on. In this way, bars can form out of small random irregularities in bed level.

1. Introduction

Beach morphology dynamics are driven by the interaction of water motion and sediment over a geological substratum. Coastal sediment transport is still poorly understood so that model representations largely rely on simplifications and parameterisations (Amoudry & Souza, 2011). At length scales comparable to the surf zone width or larger (>10–100 m), sediment transport can be conceptually decomposed into two main components. Longshore transport is driven by the surf-zone longshore current generated by breaking waves if they approach obliquely to the coast. Cross-shore transport is the main cause of the cross-shore beach profile sloping up onshore, sometimes with shore parallel sand bars. The main sources of cross-shore transport are onshore transport driven by wave asymmetry and skewness, offshore transport due to undertow (bed-return current) and downslope transport due to gravity (Fernández-Mora et al., 2015). An equilibrium bed profile is achieved if the three components are in balance. Finally, there are more contributions to sediment transport that do not fall into the longshore or cross-shore categories (e.g., those associated to rip current circulation or to low frequency motions).

On sandy coasts, beach morphology is rarely alongshore uniform. Typically, the shoreline has undulations and the nearshore sea bed features shallows and deeps alongshore. Transverse bar systems (Ribas et al., 2015) are a well-known example, encompassing a series of shallows or bars separated by deeps called rip channels (Figure 1). These systems are not only fascinating but also relevant from a scientific point of

© 2021. The Authors.

This is an open access article under the terms of the [Creative Commons Attribution-NonCommercial-NoDerivs License](https://creativecommons.org/licenses/by/4.0/), which permits use and distribution in any medium, provided the original work is properly cited, the use is non-commercial and no modifications or adaptations are made.

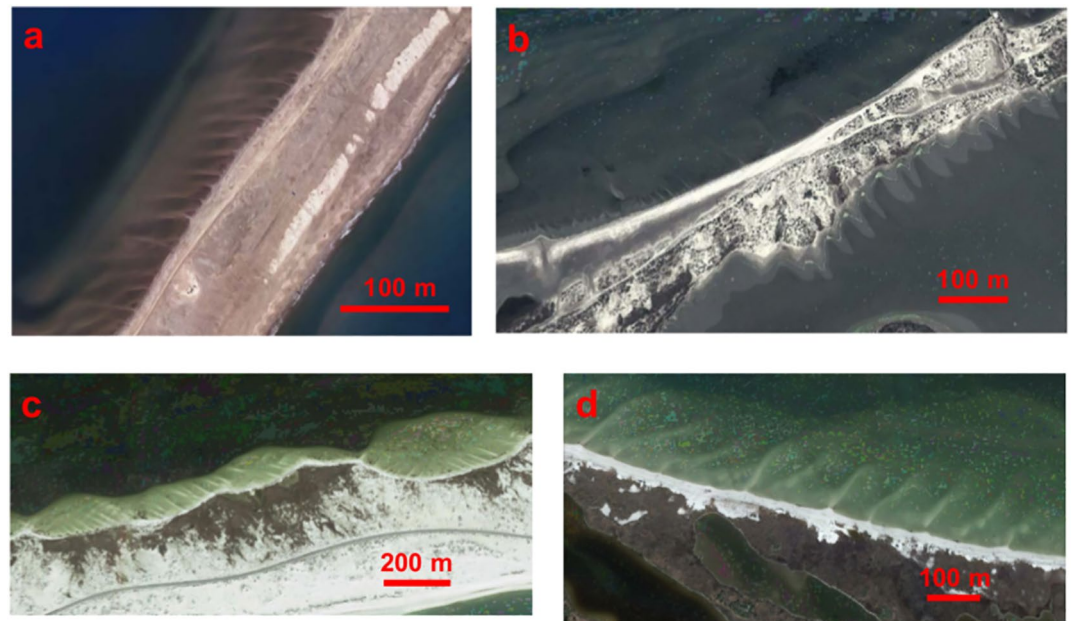


Figure 1. Shore-transverse finger sand bars in back-barrier beaches with an abundant sand supply. (a) El Trabucador, Ebro delta, Catalonia, Spain ($40^{\circ} 36' 54''$ N, $0^{\circ} 43' 44''$ E). Source: Catalan Geographic and Geologic Institute, image from 2012. (b) Beauduc Beach, Rhône Delta, France ($43^{\circ} 23' 41''$ N, $4^{\circ} 34' 35''$ E). Source: Google Earth, Maxar Technologies, image from 28/04/2010. Notice the bars (of different shape) at both sides of the barrier beach. (c) Santa Rosa Island, Florida, USA ($30^{\circ} 22' 06''$ N, $86^{\circ} 57' 32''$ W). Source: Google Earth, Terrametrics, image from 15/01/2018. (d) Horn Island, Mississippi, USA ($30^{\circ} 14' 38''$ N, $88^{\circ} 41' 06''$ W). Source: Google Earth, Landsat/Copernicus, image from 27/01/2015. The North in all plots is upward directed.

view because they give information on morphodynamic processes of which they are the occasional visible imprint. The origin of coastal rhythmic patterns has been puzzling scientists for decades but consensus has arisen that they emerge from feedbacks between hydrodynamics and morphology through sediment transport (Coco & Murray, 2007). Up to now, self-organization mechanisms related to the sediment transport due to the longshore current and the rip currents have been largely explored while possible feedbacks arising from cross-shore transport have been ignored. Several studies have unraveled feedback mechanisms based on those currents that explain the genesis of some types of rhythmic bars observed in nature (Deigaard et al., 1999; Falqués et al., 2000, 1996; Garnier et al., 2008; Murray, 2004; Reniers et al., 2004; Ribas et al., 2012, 2015, and references therein). In all these existing morphodynamic models the formation of rhythmic patterns occurs on top of a cross-shore profile that is assumed to be essentially in equilibrium. The net cross-shore transport is evaluated in a simplified way such that it only leads to a diffusive term in the equation governing bed evolution. However, the formation mechanism for transverse finger bars in low-energy environments (small maximum significant wave heights, $H_s \lesssim 1$ m, short peak periods, $T_p \lesssim 5$ s, and sandbar alongshore wavelengths of 20–200 m, Figure 1) remains mostly unexplained. In fact, observational studies on such transverse bars show that they develop preferably on gentle sloping beaches with an abundant supply of sand (Niederoda & Tanner, 1970), probably with a beach profile above equilibrium (Evans, 1938). In this situation, cross-shore transport dominates and thereby it might trigger a destabilizing mechanism instead of a damping one. Other examples are the transverse finger bars along lake shores (Evans, 1938), estuaries (Eliot et al., 2006), barrier islands (Figures 1c and 1d) (Gelfenbaum & Brooks, 2003) and delta barrier beaches (Figures 1a and 1b), including the bar system at El Trabucador back-barrier beach in the Ebro delta (Mujal-Colilles et al., 2019).

At its south west flank this delta has a long narrow spit, called El Trabucador, and its back-barrier beach is a shallow terrace of 100 m cross-shore up to 0.7 m depth, which faces the semi-enclosed Alfacs bay. The abundant and fine sand is transported from the open sea beach during overwash events. This beach is microtidal and wave energy is typically low due to the small fetch, with maximum $H_s \sim 0.6$ m during NW wind and $T_p < 3$ s. Nevertheless, wave activity is intense enough to move the fine sand over all the terrace and a

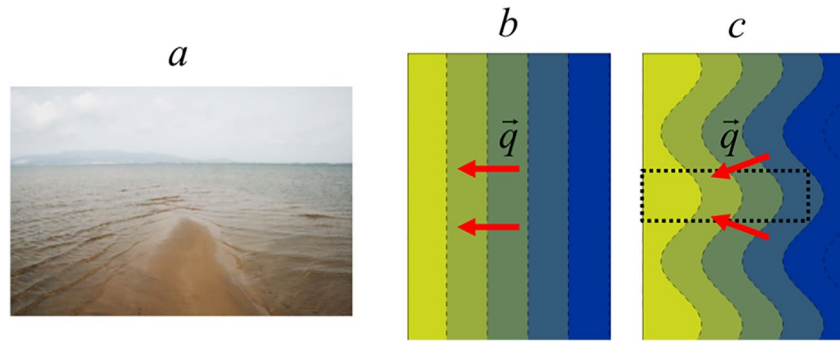


Figure 2. The morphodynamic instability mechanism: (a) wave focusing by a shore-transverse sandbar due to topographic refraction in El Trabucador back-barrier beach, (b) net onshore sediment transport for rectilinear shore-parallel depth contours above the equilibrium, and (c) rotation of the cross-shore sediment flux for curvilinear depth contours and sediment convergence over the shoals (e.g., inside the dotted rectangle). In panels (b) and (c), yellow/blue colors mean shallow/deep water, respectively.

system of transverse finger bars is often present (Figure 1a). The alongshore wavelength is variable but the average and the most frequent is 20 m (Mujal-Colilles et al., 2019). The bars are thin and elongated with a cross-shore extent up to some 60 m and they commonly open an anti-clockwise angle of 10°–40° with the shore normal. Field observations and aerial photos show that the system is persistent and dynamic. Typically, waves refract in the proximity of the bars and wave crests cross each other over the bars thereby focusing their energy there (Figure 2a). This process, very noticeable and ubiquitous, was already described by Niederröda and Tanner (1970) as an important process for the formation and maintenance of transverse finger bars in other sites.

In this paper we present a new morphodynamic self-organization mechanism based on cross-shore transport that could explain the generation of transverse finger bars in beaches with sand excess. The instability mechanism is described in section 2. Section 3 presents the model runs that confirm that, if the beach profile is above equilibrium, the cross-shore transport can generate shore-transverse sand bars similar to those observed at back-barrier beaches (Figure 1). The concluding remarks are given in section 4, along with the limitations and relevance of this theoretical study.

2. The New Instability Mechanism

To describe the instability mechanism we consider an idealized beach with a rectilinear shoreline and an alongshore uniform bathymetry. We focus on the case where waves approach normally to the coast. Let us assume a cross-shore beach profile with a slope that is gentler than the equilibrium slope at each cross-shore position. Thereby, the gravity-driven transport is small and the net depth-averaged cross-shore sediment flux, \bar{q} , is dominated by wave asymmetry and skewness, hence onshore directed (Figure 2b). Assume now a shoal breaking the alongshore uniformity. The waves propagating in the vicinity of the shoal will refract so that the wave crests at both sides of the shoal will veer toward the shallowest part (Figure 2a). As a result, the sediment flux direction will also change, delivering sediment to the shoal so that it will tend to grow and a positive feedback will occur (Figure 2c). On the contrary, if the cross-shore profile is steeper than the equilibrium profile, the net cross-shore transport is dominated by gravity, hence seaward directed, and the situation is just the opposite. Now, on the flanks of the incipient shoal, where the slopes are steepest, downslope transport will be enhanced, causing a divergence of sediment transport away from the shoal.

The instability mechanism can be mathematically described with an idealized morphodynamic equation associated with cross-shore transport. This also facilitates understanding the essential differences with the usual approach where cross-shore transport plays a diffusive role. We consider a Cartesian coordinate system (x, y, z) , x pointing seawards, y along the shoreline and z upwards, $z = 0$ being the mean sea level. We represent the cross-shore sediment transport as

$$\bar{q} = q_w \frac{\bar{k}}{k} - \gamma \nabla z_b. \quad (1)$$

It only contains the wave-driven and the gravitational transports because this is the simplest way to capture the essence of the new instability. Here, q_w is the onshore wave-driven transport module, \vec{k} is the wavenumber vector, $\gamma > 0$ is a wave stirring factor and $z = z_b(x, y, t)$ is the bed level. Other contributions to cross-shore transport, like undertow or infragravity waves, or the sediment transport by currents are ignored in this section. We consider a rectilinear shoreline, $y = 0$, and an alongshore uniform bathymetry, $z_b = Z(x)$, as a reference beach state, not necessarily in equilibrium. The local reference beach slope is $\beta(x) = -dZ(x)/dx$. In the reference state we assume shore-normal incident monochromatic waves.

Let us consider now a small alongshore irregularity on the reference state, $h(x, y, t)$, so that $z_b(x, y, t) = Z(x) + h(x, y, t)$. It is important to realize that although h is assumed to be infinitesimal, the total perturbation with respect to the equilibrium, $Z(x) - Z_e(x) + h(x, y, t)$ is not. Let $\theta(\phi)$ be the small angle between $\nabla z_b(\vec{k})$ and the $-x$ axis, that is,

$$\nabla z_b = |\nabla z_b|(-\cos\theta\hat{e}_x + \sin\theta\hat{e}_y), \quad \vec{k} = k(-\cos\phi\hat{e}_x + \sin\phi\hat{e}_y), \quad (2)$$

where \hat{e}_x, \hat{e}_y are the unit vectors along the x, y axes. Introducing this in the sediment transport one obtains

$$\vec{q} = q_w^0(-\cos\phi\hat{e}_x + \sin\phi\hat{e}_y) + \gamma^0\beta\hat{e}_x - \gamma^0\nabla h, \quad (3)$$

where q_w^0 and γ^0 are the magnitudes of the wave-driven transport and the stirring in the reference state, respectively. The perturbations in q_w and γ have been here neglected for simplicity, as done in most morphodynamic models (Ribas et al., 2015). Then, by keeping only zero and first order terms,

$$\vec{q} = Q\hat{e}_x + q_w^0\phi\hat{e}_y - \gamma^0\nabla h, \quad (4)$$

with $Q = \gamma^0\beta - q_w^0$ being the net transport in the reference state. Due to topographic refraction, the wave fronts tend to become parallel to the depth contours. We can therefore assume $\phi = \mu\theta$ with $0 < \mu(x, y) < 1$. In fact, $\phi(x, y)$ is not a local function of $\theta(x, y)$, since it depends on the whole wave refraction from offshore to the (x, y) location, but for our purpose and for small angles this assumption seems reasonable. Furthermore, to first order, Equation 2 leads to

$$\theta = \frac{1}{\beta} \frac{\partial h}{\partial y}. \quad (5)$$

Finally, by invoking the sediment conservation equation,

$$\frac{\partial z_b}{\partial t} + \frac{1}{1-p} \nabla \cdot \vec{q} = 0, \quad (6)$$

with p being the bed porosity, the following morphodynamic governing equation is obtained

$$(1-p) \frac{\partial h}{\partial t} = \frac{\partial}{\partial x} \left(\gamma^0 \frac{\partial h}{\partial x} \right) + \frac{\partial}{\partial y} \left(\gamma^0 (1-\alpha) \frac{\partial h}{\partial y} \right) - \frac{dQ}{dx}, \quad (7)$$

where $\alpha = \mu q_w^0 / (\gamma^0 \beta)$. This is a diffusion equation where the cross-shore and the alongshore diffusivities are γ^0 and $\gamma^0(1-\alpha)$, respectively. If the reference state is an equilibrium state, $Q = 0$. Moreover, if wave refraction is neglected, $\mu = \alpha = 0$, and both diffusivities in Equation 7 are equal and positive. This is the standard approach in which any bathymetric perturbation tends to be damped (Ribas et al., 2015). Now, including wave refraction reduces the alongshore diffusivity but, if the reference state is an equilibrium one, the alongshore diffusivity is still positive ($0 < \alpha < 1$). However, if the reference profile is less steep than the equilibrium profile, the net cross-shore transport is positive, $q_w^0 > \gamma^0\beta$, and the alongshore diffusivity may become negative ($\alpha > 1$). In this case, alongshore irregularities can grow due to a morphodynamic instability.

3. Morphodynamic Model Runs

3.1. Brief Model Description

To study in more detail how the instability mechanism works and is able of generating alongshore rhythmic morphology we use the Q2Dmorfo model (Arriaga et al., 2017). This model computes the evolving bathymetry in a rectangular domain under a given wave forcing. The main inputs are the initial bathymetry, the wave forcing and an assumed equilibrium beach profile. From this, the model computes the wave field inside the domain and the sediment flux, and it updates the bathymetry at each time step from the depth-averaged sediment conservation Equation 6. The model is similar to other existing 2DH morphodynamic models except that it computes the sediment flux directly from the wave field in a parametric way without resolving the surf zone hydrodynamics. By neglecting some important surf zone processes (like rip currents) it is able to describe the large scale coastal evolution at time scales of decades-centuries. It has also been validated with observations (Arriaga et al., 2017). Although we are here interested in length scales much smaller than those for which the model was designed, we use it for two reasons. First, it describes the cross-shore transport as proportional to the deviation of the local beach slope with respect to the equilibrium one. Second, it filters out the rip current circulation which is another known factor of alongshore rhythmic morphology. Therefore, the mechanism associated to the cross-shore transport can be analyzed in isolation.

The model is here briefly described, mainly indicating how the sediment fluxes are calculated from the wave field. More details can be found in Arriaga et al. (2017). We use the same coordinate system introduced in section 2 and a computational domain $0 \leq x \leq L_x$, $0 \leq y \leq L_y$, including emerged and submerged beach. The depth-integrated sediment flux is decomposed into three components,

$$\bar{q} = \bar{q}_L + \bar{q}_C + \bar{q}_D. \quad (8)$$

The first one is a parameterization of the longshore sediment flux driven by the breaking waves. The second one is the cross-shore transport and reproduces the tendency of the beach to evolve toward the equilibrium profile. The third term is an alongshore diffusive transport to account for the hydrodynamic smoothing of small scale bathymetric noise. For an undulating coast, the cross-shore and alongshore directions loose the clear meaning they have for a rectilinear coast. However their meaning can be recovered from the mean trend of the bathymetric contours if the small scale bathymetric features are filtered out. Also, these averaged contours are those felt by wave propagation and transformation. Therefore, from the actual bathymetry, $z_b(x, y, t)$, an averaged bathymetry, $\bar{z}_b(x, y, t)$, is defined by using a running average in a rectangular window of size a_x and a_y , which must be at least of the order of the wavelength. Then, we define the local mean “cross-shore” direction by the unit vector

$$\hat{n} = -\frac{1}{|\nabla \bar{z}_b|} \nabla \bar{z}_b. \quad (9)$$

The cross-shore transport in Equation 8 is proportional to the difference between the local equilibrium slope, $\beta_e(D)$, and the actual slope in the local cross-shore direction,

$$\bar{q}_C = -\gamma_C(\hat{n} \cdot \nabla z_b + \beta_e)\hat{n}. \quad (10)$$

The water depth is $D = -z_b$ and $\gamma_C(D)$ is a wave stirring factor, decreasing seawards. The depth where γ_C is 2% of its shoreline value is the depth of closure, D_c . Note that Equation 10 implies that the wave-driven transport points exactly in the up-slope direction of the averaged bathymetry. In the framework of section 2, this is equivalent to the limit case $\mu = 1$, that is, $\phi = \theta$.

Model runs are based on the geometry and typical wave conditions at El Trabucador back-barrier beach. A rectangular domain $L_x = 200$ m (cross-shore), $L_y = 600$ m (longshore), with a dry beach width of 20 m. As equilibrium profile, we consider a shifted Dean profile (Falqués & Calvete, 2005),

$$Z_e(x) = -B\left((x + x_0)^{2/3} - x_0^{2/3}\right). \quad (11)$$

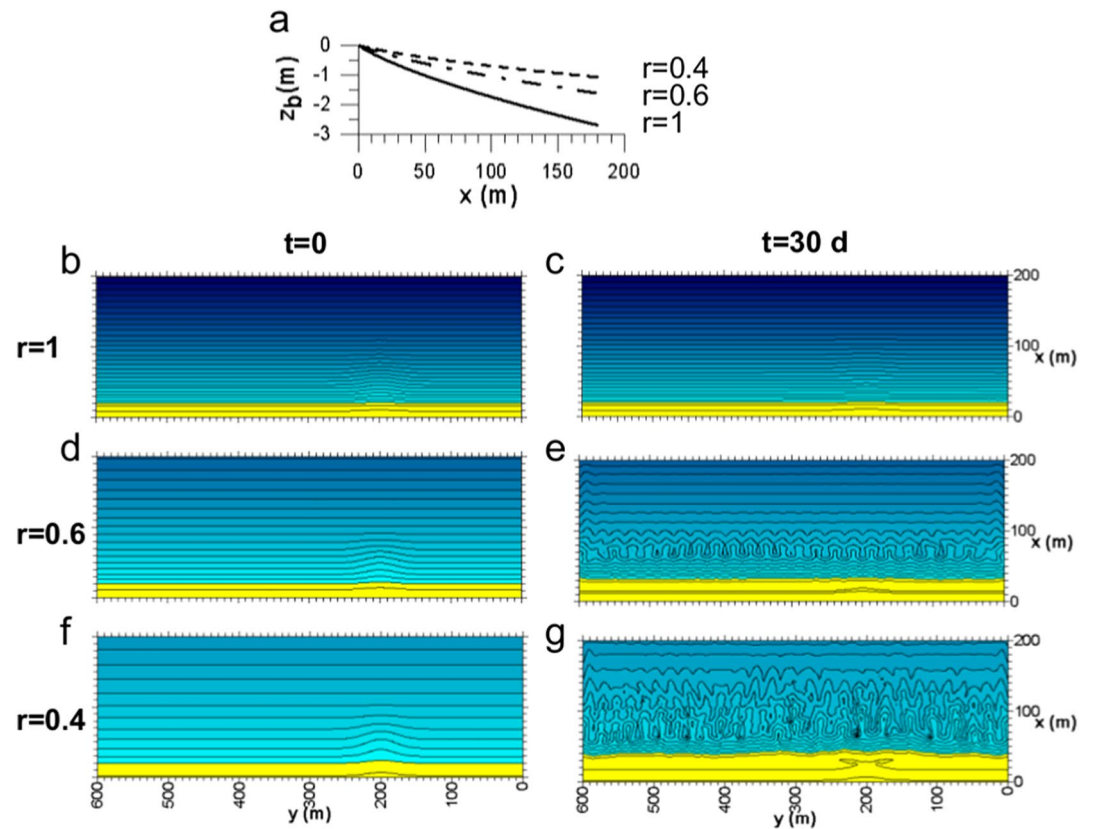


Figure 3. Sensitivity to the initial beach slope: (a) Initial profile for $r = 1$ in solid line (which is also the equilibrium profile), and for $r = 0.6$ and $r = 0.4$, and (b)–(g) Q2Dmorfo result for the three r values. Panels (b), (d) and (f) are the initial bathymetry and panels (c), (e) and (g) are the bathymetries at $t = 30$ days. Yellow and blue colors represent the emerged and submerged beach, respectively, and depth contours are plotted every 0.1 m.

The parameters, $B = 0.095 \text{ m}^{1/3}$ and $x_0 = 9.42 \text{ m}$, are chosen to obtain a shoreline slope $\beta_s = 0.03$ and to approximate a Dean profile far from the shoreline, $Z_d = -Ax^{2/3}$, with $A = 0.084 \text{ m}^{1/3}$. This A value is consistent with a sediment grain size $d_{50} \approx 0.15 \text{ mm}$ (Dean & Dalrymple, 2002). The imposed values for β_s and d_{50} are obtained from El Trabucador data (Mujal-Colilles et al., 2019). The initial bathymetry for the model runs is

$$z_b(x, y, 0) = rZ_e(x) + h(x, y), \quad (12)$$

where $h(x, y)$ is a small perturbation localized at $y = 200 \text{ m}$ (Figures 3b, 3d and 3f) and r controls whether the initial profile is above ($r < 1$) or below ($r > 1$) equilibrium (Figure 3a). A value $r \approx 0.4$ is obtained by fitting a shifted Dean profile to the observed profile at El Trabucador, and it is used as default value. This means that the observed profile is clearly above the equilibrium profile that would correspond to its grain size. As default wave forcing we use constant wave conditions characteristic from El Trabucador, $H_s = 0.28 \text{ m}$, $T_p = 2 \text{ s}$ (Mujal-Colilles et al., 2019), and shore-normal incidence, $\theta = 0$. The default bathymetric smoothing box is $a_x = 3 \text{ m}$ and $a_y = 10 \text{ m}$, and the closure depth is estimated out of the data, $D_c = 0.8 \text{ m}$. The spatial grid is defined by $dx = 0.5 \text{ m}$ and $dy = 1.5 \text{ m}$ and the time step is $dt = 1.7 \text{ s}$.

3.2. Model Results

For $r = 1$ the initial perturbation tends to smooth out and the bathymetric contours become rectilinear and parallel to the shoreline (Figures 3b and 3c). The initial morphology is clearly stable. In contrast, for $r = 0.4$ undulations develop in the depth contours (Figures 3f and 3g). Quite rapidly, the amplitude of the undulations increases and a complex bathymetry encompassing shore-transverse bars appears in the shoaling zone. Thus, the initial morphology is clearly unstable. At some spots, the morphology is relatively regular

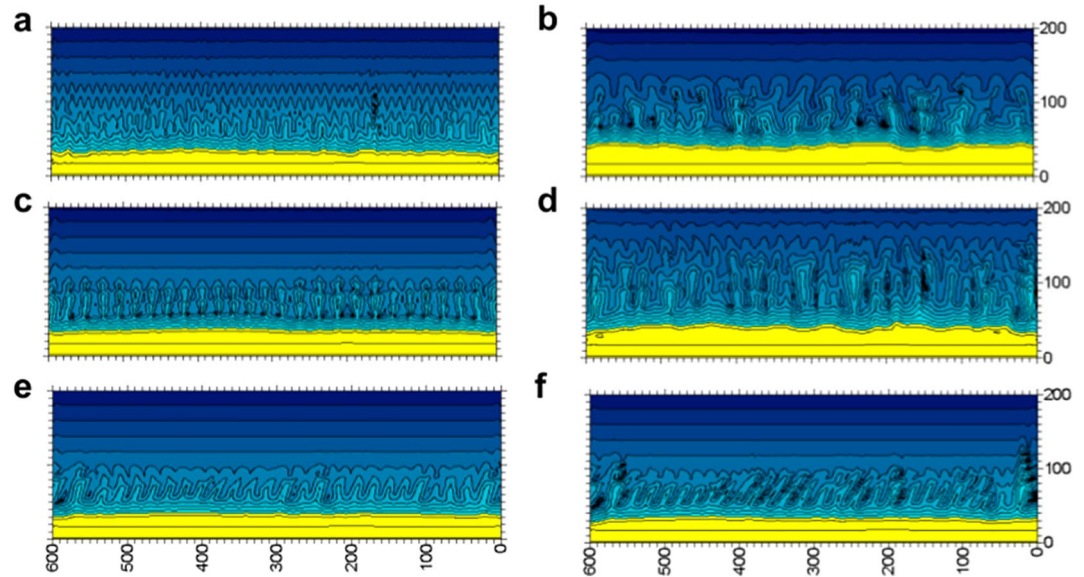


Figure 4. Q2Dmorfo result for (a) $a_y = 5$ m and (b) $a_y = 20$ m, both at $t = 20$ days, for (c) $D_c = 0.6$ m and (d) $D_c = 1$ m, both at $t = 19$ days, and for (e) $\theta = 10^\circ$ and (f) $\theta = 20^\circ$, both at $t = 2$ days. The other parameters have their default values. Yellow and blue colors represent the emerged and submerged beach, respectively, and depth contours are plotted every 0.1 m. In case of oblique wave incidence, waves came from the right on the plot.

but at others it is quite complex with several length scales. However, a dominant alongshore length scale $L \approx 25$ m becomes apparent. Also, the shoreline progrades, which is consistent with the beach being under accretive conditions. A detailed description of the time evolution of the morphology in the default case can be found in the Supporting Information S1. For $r = 0.5$ – 0.7 something similar occurs but at a slower rate as r increases. For $r = 0.7$ only some weak undulations in the depth contours have developed after 30 days. In contrast, the behavior for $r = 0.8$ is similar to $r = 1$. Thus, it is found that the instability develops only if the profile is above equilibrium but with a certain threshold.

To test whether the instability is a numerical artifact, the sensitivity to the numerical parameters is investigated. Little sensitivity is found when varying dy between 0.5 and 1.5 m or changing the size of the domain, from $L_y = 300$ – 600 m. Also, results do not depend on the initial perturbation (three cases have been analyzed, see the Supporting Information S1 for details). The particular morphology is somewhat different, but the qualitative behavior is the same. The robustness of the results when varying dt is also shown in the Supporting Information S1. The sensitivity to the averaging box size, a_x , a_y , has been carefully examined. It is found that a_x hardly influences the results but a_y has a strong influence on the shape and wavelength of the transverse bar system. For small a_y the morphology is quite complex and noisy, and the spacing between the bars is small. In contrast, as a_y increases, it becomes smoother and the spacing increases (see Figures 4a and 4b). Indeed, it is found that wavelength increases (roughly) linearly with a_y (see the Supporting Information S1 for details). For $a_y > 50$ m, bars do not grow inside the domain. The dependence of the results on a_y is discussed in section 4.

Regarding wave conditions, the ranges $H_s = 0.14$ – 0.42 m and $T_p = 1$ – 3 s are tested and the basic instability mechanism does not change. The wave height has some influence on the bars, higher waves causing longer and more alongshore spaced bars. The wave period has no direct influence, but it has an important indirect influence through a_y , as will be discussed in section 4 (more details about the effect of H_s and T_p in the Supporting Information S1). D_c and θ have more influence. The values $D_c = 0.6$ – 1.2 m have been examined and its primary influence is an increase of the cross-shore length of the bars with increasing D_c (Figures 4c and 4d). For oblique wave incidence, bars grow faster and are obliquely orientated, pointing into the direction of wave incidence (Figures 4e and 4f). Morphodynamic noise appears much sooner than for shore normal wave incidence and the model breaks down earlier (for example at $t = 15$ days for $\theta = 10^\circ$ but as soon as $t = 2$ days for $\theta = 40^\circ$).

4. Final Remarks

The resulting onshore sediment transport on beaches that are significantly shallower than the equilibrium bathymetric profile can produce an instability that breaks the alongshore uniformity. The instability occurs because wave refraction rotates the wave fronts toward the growing transverse bars so that the onshore transport also veers and causes flux convergence over the bars. This mechanism can explain the common existence of transverse finger bars in shallow areas with an abundant supply of sand in delta barrier beaches, barrier islands and estuaries (Figure 1). A beach profile less steep than the equilibrium one can occur when overwash across a barrier deposits sediment at a rate greater than the rate at which small back barrier waves can sweep it in back to the beach. A sediment excess (with respect to equilibrium) could also occur in open beaches in case of, for example, persistent convergence in alongshore transport.

It is remarkable that, although the present modeling approach is just meant to capture the essence of the instability in a qualitative way, the modeled morphology bears a reasonable similitude with the transverse bars shown in Figure 1. In particular, they extend perpendicularly to the shoreline inside the shoaling zone, with cross-shore spans significantly larger than their wavelengths. Moreover, the model application to El Trabucador gives emerging length scales consistent with those measured in this site. The dominant alongshore spacing between the bars, L , increases linearly with the alongshore length of the smoothing box, a_y . The latter must be of the order of the minimum alongshore length scale of the bathymetric features that can affect wave refraction, which is difficult to ascertain but must be of the order of the wavelength of the wave forcing. At the water depths $D \approx 0.4\text{--}0.6$ m where the bars form, waves with $T_p = 2\text{--}3$ s have wavelengths in the range 4–7 m which would be an appropriate range for a_y . Alongshore wavelengths $L \approx 16\text{--}19$ m are then obtained, which are consistent with the most frequent bar spacing at El Trabucador (Mujal-Colilles et al., 2019). This also suggests that the alongshore bar spacing of such type of transverse bars would generally scale with the wavelength of the waves, with a factor ~ 3 . Regarding the cross-shore extent of the bars, it is controlled by the depth of closure, D_c , and a value of about 60–90 m is found for this site (the maximum observed is about 60 m). Finally, we should stress that the wave refraction process over the bars, which is essential to the instability, is also commonly observed at El Trabucador back-barrier beach (Mujal-Colilles et al., 2019).

Although we have focused here on illustrating the capability of the present mechanism to generate transverse finger bars in areas of sand excess, it could also influence the down-state sequence under accretive conditions in any beach (Wright & Short, 1984) and the development of, for example, crescentic bars (Dubarbier et al., 2017). This should be investigated with a surf (and shoaling) zone morphodynamic model incorporating a parameterization of cross-shore transport capable of accounting for the present instability mechanism in open ocean beach environments.

The instability concept had been applied to explain the formation of beach cusps (Dodd et al., 2008), crescentic bars (Garnier et al., 2008), shore-transverse bars (Ribas et al., 2012), shoreline sand waves and large scale cusped features (and spits) (Ashton et al., 2001). In all these cases the morphological features develop out of an equilibrium state, that is, time invariant, both in the case of linear or nonlinear analysis. In contrast, the new instability develops from a morphology which is necessarily not an equilibrium state. In this sense, it is a finite-amplitude instability, that is, it can not be captured by the usual linear stability analysis of an equilibrium morphology. Finite-amplitude instabilities are common in other fields of Physics (Drazin & Reid, 1981; Eckhardt et al., 2007; Grossmann, 2000) but, to our knowledge, they had not been found so far in coastal geomorphology.

Data Availability Statement

Datasets from El Trabucador back-barrier beach are included in the article Mujal-Colilles et al. (2019).

Acknowledgments

This research is part of the Spanish Government projects CTM2015-66225-C2-1-P and RTI2018-093941-B-C33 (MINECO/FEDER). Finally, the constructive comments of Prof. Brad Murray and Dr. Ryan P. Mulligan helped to improve the quality of this paper.

References

- Amoudry, L. O., & Souza, A. J. (2011). Deterministic coastal morphological and sediment transport modeling: A review and discussion. *Reviews of Geophysics*, 49(2). <https://doi.org/10.1029/2010RG000341>
- Arriaga, J., Rutten, J., Ribas, F., Ruessink, B., & Falqués, A. (2017). Modeling the longterm diffusion and feeding capability of a mega-nourishment. *Coastal Engineering*, 121, 1–13. <https://doi.org/10.1016/j.coastaleng.2016.11.011>

- Ashton, A., Murray, A. B., & Arnault, O. (2001). Formation of coastline features by large-scale instabilities induced by high-angle waves. *Nature*, *414*, 296–300. <https://doi.org/10.1038/35104541>
- Coco, G., & Murray, A. B. (2007). Patterns in the sand: From forcing templates to self-organization. *Geomorphology*, *91*, 271–290. <https://doi.org/10.1016/j.geomorph.2007.04.023>
- Dean, R. G., & Dalrymple, R. A. (2002). *Coastal processes*. Cambridge University Press.
- Deigaard, R., Dronen, N., Fredsoe, J., Jensen, J. H., & Jørgensen, M. P. (1999). A morphological stability analysis for a long straight barred coast. *Coastal Engineering*, *36*(3), 171–195. [https://doi.org/10.1016/s0378-3839\(99\)00005-8](https://doi.org/10.1016/s0378-3839(99)00005-8)
- Dodd, N., Stoker, A., Calvete, D., & Sriariyawat, A. (2008). On beach cusp formation. *Journal of Fluid Mechanics*, *597*, 145–169. <https://doi.org/10.1017/s002211200700972x>
- Drazin, P. G., & Reid, W. H. (1981). *Hydrodynamic stability*. Cambridge University Press.
- Dubarbier, B., Castelle, B., Ruessink, G., & Mariou, V. (2017). Mechanisms controlling the complete accretionary beach state sequence. *Geophysical Research Letters*, *44*, 5645–5654. <https://doi.org/10.1002/2017GL073094>
- Eckhardt, B., Schneider, T. M., Hof, B., & Westerweel, J. (2007). Turbulence transition in pipe flow. *Annual Review of Fluid Mechanics*, *39*, 447–468. <https://doi.org/10.1146/annurev.fluid.39.050905.110308>
- Eliot, M. J., Travers, A., & Eliot, I. (2006). Morphology of a Low-Energy Beach, Como Beach, Western Australia. *Journal of Coastal Research*, *22*(1), 63–77. <https://doi.org/10.2112/05a-0006.1>
- Evans, O. F. (1938). The classification and origin of beach cusps. *The Journal of Geology*, *46*, 615–627. <https://doi.org/10.1086/624662>
- Falqués, A., & Calvete, D. (2005). Large scale dynamics of sandy coastlines. Diffusivity and instability. *Journal of Geophysical Research*, *110*, C03007. <https://doi.org/10.1029/2004JC002587>
- Falqués, A., Coco, G., & Huntley, D. A. (2000). A mechanism for the generation of wave-driven rhythmic patterns in the surf zone. *Journal of Geophysical Research*, *105*(C10), 24071–24087. <https://doi.org/10.1029/2000jc900100>
- Falqués, A., Montoto, A., & Iranzo, V. (1996). Bed-flow instability of the longshore current. *Continental Shelf Research*, *16*(15), 1927–1964. [https://doi.org/10.1016/0278-4343\(96\)00031-3](https://doi.org/10.1016/0278-4343(96)00031-3)
- Fernández-Mora, A., Calvete, D., Falqués, A., & Swart, de, H. E. (2015). Onshore sandbar migration in the surf zone: New insights into the wave-induced sediment transport mechanisms. *Geophysical Research Letters*, *42*(8), 2869–2877. <https://doi.org/10.1002/2014GL063004>
- Garnier, R., Calvete, D., Falqués, A., & Dodd, N. (2008). Modeling the formation and the long-term behavior of rip channel systems from the deformation of a longshore bar. *Journal of Geophysical Research*, *113*, C07053. <https://doi.org/10.1029/2007JC004632>
- Gelfenbaum, G., & Brooks, G. R. (2003). The morphology and migration of transverse bars off the west-central florida coast. *Marine Geology*, *200*, 273–289. [https://doi.org/10.1016/s0025-3227\(03\)00187-7](https://doi.org/10.1016/s0025-3227(03)00187-7)
- Grossmann, S. (2000). The onset of shear flow turbulence. *Reviews of Modern Physics*, *72*(2), 603–618. <https://doi.org/10.1103/revmodphys.72.603>
- Mujal-Colilles, A., Grifoll, M., & Falqués, A. (2019). Rhythmic morphology in a microtidal low-energy beach. *Geomorphology*, *334*, 151–164. <https://doi.org/10.1016/j.geomorph.2019.02.037>
- Murray, A. B. (2004). Rip channel development on nonbarred beaches: The importance of a lag in suspended-sediment transport. *Journal of Geophysical Research*, *109*, C04026. <https://doi.org/10.1029/2002JC001581>
- Niederoda, A. W., & Tanner, W. F. (1970). Preliminary study on transverse bars. *Marine Geology*, *9*, 41–62.
- Reniers, A. J. H. M., Roelvink, J. A., & Thornton, E. B. (2004). Morphodynamic modeling of an embayed beach under wave group forcing. *Journal of Geophysical Research*, *109*, C01030. <https://doi.org/10.1029/2002JC001586>
- Ribas, F., Falqués, A., Swart, de, H. E., Dodd, N., Garnier, R., & Calvete, D. (2015). Understanding coastal morphodynamic patterns from depth-averaged sediment concentration. *Reviews of Geophysics*, *53*, 362–410. <https://doi.org/10.1002/2014RG000457>
- Ribas, F., Swart, de, H. E., Calvete, D., & Falqués, A. (2012). Modeling and analyzing observed transverse sand bars in the surf zone. *Journal of Geophysical Research*, *117*, F02013. <https://doi.org/10.1029/2011JF002158>
- Wright, L. D., & Short, A. D. (1984). Morphodynamic variability of surf zones and beaches: A synthesis. *Marine Geology*, *56*, 93–118. [https://doi.org/10.1016/0025-3227\(84\)90008-2](https://doi.org/10.1016/0025-3227(84)90008-2)